Theoretical and Applied Fracture Mechanics 125 (2023) 103926

Contents lists available at ScienceDirect

Theoretical and Applied Fracture Mechanics

journal homepage: www.elsevier.com/locate/tafmec

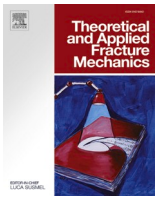

Analysis of additively manufactured notched PLA plates using failure assessment diagrams

Sergio Cicero [a,*], Sergio Arrieta [a], Marcos Sánchez [a], Laura Castanon-Jano [b]

[a] LADICIM (Laboratory of Materials Science and Engineering), Universidad de Cantabria, E.T.S. de Ingenieros de Caminos, Canales y Puertos, Av/ Los Castros 44, Santander, 39005 Cantabria, Spain
[b] Department of Transport, Projects and Process Technology, University of Cantabria, 39005 Santander, Spain

ARTICLE INFO

Keywords:
Additively manufactured
PLA
Notch
Failure assessment diagram
Theory of critical distances

ABSTRACT

This paper provides a methodology for the estimation of the load-bearing capacity of additively manufactured (AM) PLA plates containing different types of notches (U-notches, V-notches and holes). The methodology is based on the use of Failure Assessment Diagrams (FADs), which are the main fracture-plastic collapse assessment tool provided by structural integrity assessment procedures, such as BS7910 and API 579-1/ASME FFS-1. When analyzing notch-type defects, the FAD methodology requires the application of a notch correction which, in this work, is based on the Theory of Critical Distances (TCD) and the Creager-Paris stress distribution ahead of the crack-tip. The results show that the FAD methodology can be efficaciously applied in this AM polymer, providing safe conservative estimations of critical loads in U-notched and V-notched plates, and accurate slightly unsafe estimations in plates with central hole. The cracking behavior in the different tested plates is a complex procedure generated by a combination of filament failures and debonding processes.

1. Introduction

The analysis of failure processes in the presence of crack-like defects is generally performed by applying the assessment criteria provided by structural integrity assessment procedures (e.g., FINTET FFS [1–2], BS7910 [3], API 579-1/ASME FFS-1 [4]), most of which are based on Failure Assessment Diagrams (FADs). These diagrams provide a simultaneous analysis of fracture and plastic collapse processes through two normalized parameters, K_r and L_r:

$$K_r = \frac{K_I}{K_{mat}} \tag{1}$$

$$L_r = \frac{P}{P_L} = \frac{\sigma_y}{\sigma_{ref}} \tag{2}$$

K_I is the stress intensity factor, K_{mat} is the material fracture resistance in terms of stress intensity factor units, P is the applied load in the component being assessed, P_L is the limit load, σ_y is the material yield stress and σ_{ref} is the reference stress. Consequently, K_r evaluates the (cracked) component against fracture, whereas L_r evaluates the (cracked) component against plastic collapse. K_r and L_r establish the coordinates of the resulting assessment point, which have to be compared with the critical conditions defined by the Failure Assessment Line (FAL). Thus, when the assessment point is located above the FAL, the component is considered to be under unsafe conditions, whereas if the assessment point is located within the area defined by the FAL and the coordinate axes, the component is considered to be under safe conditions. Lastly, the failure condition is defined when the assessment point lies exactly on the FAL [1–4]. Assessment procedures provide analytical solutions for K_I and P_L (or σ_{ref}) for a wide variety of practical situations.

However, there are abundant situations where the defects affecting the integrity of a given component or structure are not crack-like defects. Some examples would be mechanical damage, corrosion defects, fabrication defects, holes, corners, weld toes, etc. When such defects are blunt, it may be overly conservative to proceed on the hypothesis that they behave like cracks and to apply fracture mechanics criteria. The literature reveals (e.g, [5–11]) that components with non-sharp defects (i.e., notches) exhibit an apparent fracture toughness (K^N_{mat}) which is greater than the fracture toughness obtained in cracked conditions, with a direct impact on the load-bearing capacity of the component being analyzed. The analysis of the fracture behavior of notched materials can be performed using different criteria (e.g., [5,12–14]), among which the

* Corresponding author.
E-mail address: ciceros@unican.es (S. Cicero).

https://doi.org/10.1016/j.tafmec.2023.103926
Received 3 April 2023; Received in revised form 4 May 2023; Accepted 4 May 2023
Available online 9 May 2023

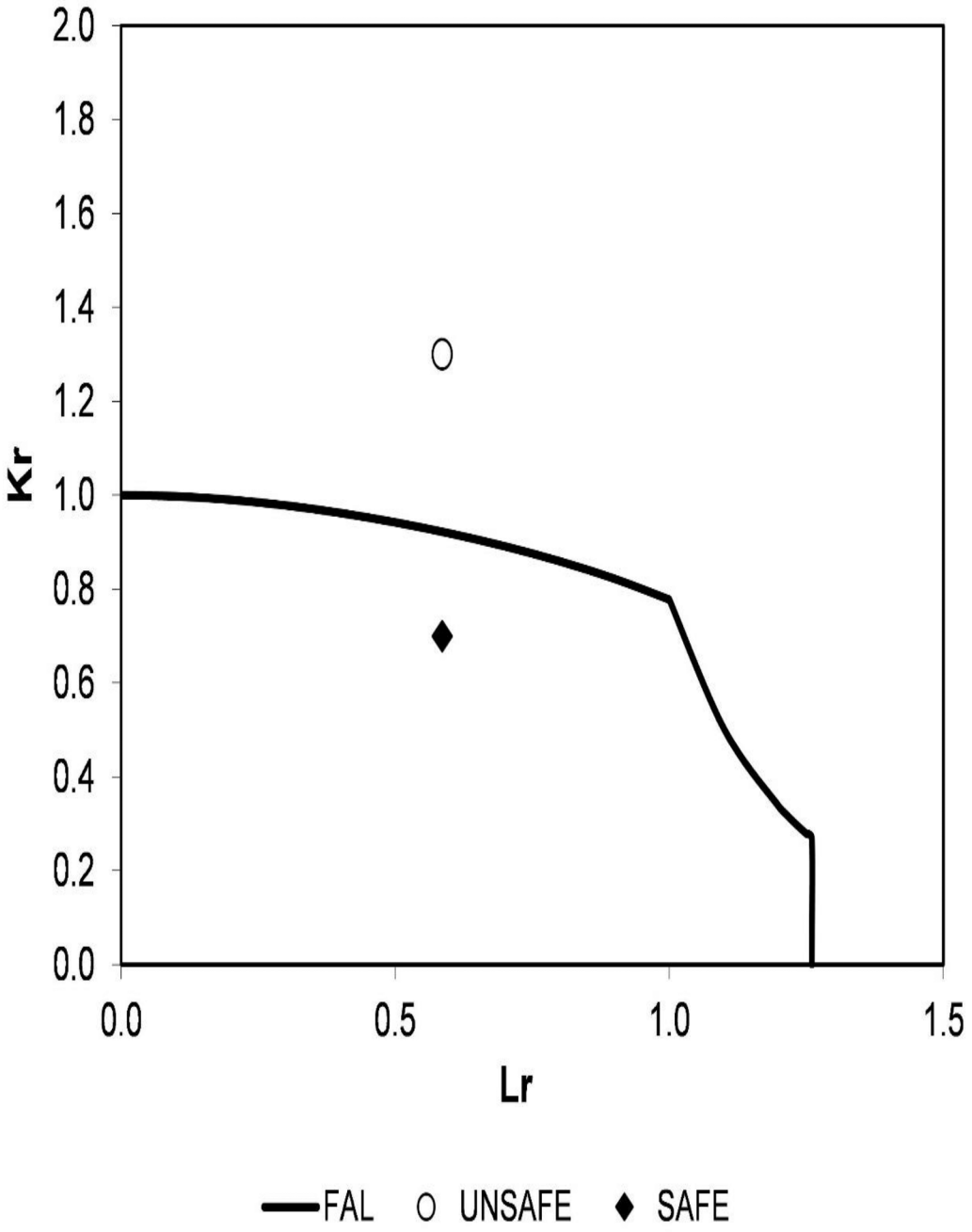

Fig. 1. Example of FAD assessment.

Theory of Critical Distances (TCD) has been extensively explained and validated in [5], and may be used to generate structural integrity assessment criteria for components containing notch-type defects, as proposed in [11] through the combination of FADs and the TCD.

Moreover, the above-mentioned structural integrity assessment procedures address the analysis of metallic materials, but do not cover non-metallic materials which, on the other hand, are being incorporated into structural applications. Some research has provided FAD assessments of non-metallic materials containing cracks (e.g., [15,16]) but, to the knowledge of the authors, there is just one work [17] analyzing the use of FADs in the assessment of 3D printed (fused deposition modelling) polymers, with such research being strictly focused on typical (SENB) fracture mechanics specimens. In this sense, additive manufacturing (AM), and particularly fused deposition modelling (FDM), is a growing technology that allows complex geometries to be generated using a relatively simple method, but the use of FDM materials in structural applications requires the development of specific structural integrity assessment criteria.

This work provides an approach to the structural integrity analysis of FDM PLA plates containing notches. With this aim, section 2 provides a brief description of the FAD methodology when assessing notch-type defects, section 3 provides a description of both the basic characterization of the PLA material being analyzed and the experimental program performed on the PLA notched plates, section 4 gathers the results and

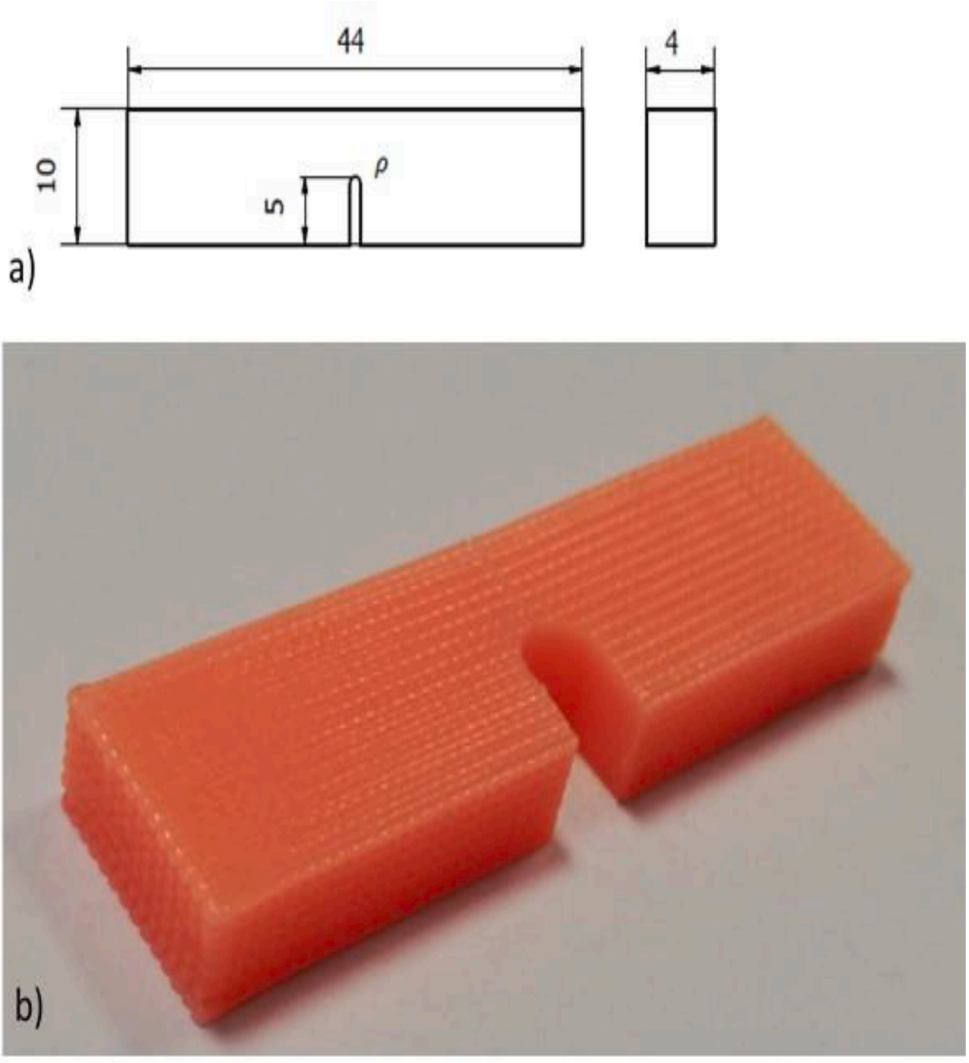

Fig. 2. PLA SENB specimens containing U-notches. a) Schematic of a generic specimen; b) image of a particular specimen, with notch radius (ρ) = 2.0 mm, and raster orientation 0/90. Dimensions in mm.

the discussion, and section 5 outlines the main conclusions.

2. Theoretical background

Fig. 1 shows an example of a FAD assessment with two different situations: a component with the assessment point located within the area defined by the coordinate axes and the Failure Assessment Line (FAL), corresponding to a safe situation; a component whose assessment point lies above the FAL, corresponding to an unsafe situation.

The FAL follows expressions which are functions of L_r:

$$K_r = f(L_r) \tag{3}$$

The different $f(L_r)$ functions are actually plasticity corrections to the linear-elastic fracture assessment ($K_I = K_{mat}$), whose exact analytical solution is:

$$f(L_r) = \sqrt{\frac{J_e}{J}} \tag{4}$$

where J is the applied J-integral and J_e is its elastic component. In practice, structural integrity assessment procedures (e.g., [1–4]) provide approximate solutions to (4), which are defined through the tensile properties of the material. These approximate solutions are generally provided hierarchically, defining different levels on which the more defined the material stress–strain curve, the more approximate are such solutions to equation (4).

Concerning the TCD, it comprises different methodologies (point method, line method, area method, etc.) [5] which, in the context of fracture assessments, make use of a material length parameter (the critical distance, L) together with the material fracture toughness. This work is focused on the line method (LM), which assumes that fracture occurs when the average stress along a distance equal to 2L (starting from the defect tip), reaches the inherent strength, σ_0:

$$\frac{1}{2L}\int_0^{2L} \sigma(r)dr = \sigma_0 \tag{5}$$

L is defined by equation (6):

$$L = \frac{1}{\pi}\left(\frac{K_{mat}}{\sigma_0}\right)^2 \tag{6}$$

The LM can be applied to the analysis of the load-bearing capacity of components containing notches. Moreover, the LM may easily generate predictions of the apparent fracture toughness (K^N_{mat}) exhibited by components containing U-shaped notches [5] by combining equation (5) with the stress distribution on the notch tip provided by Creager and Paris [18] (see [5] for details), which is equal to that ahead of the crack tip but displaced a distance equal to ρ/2 along the x-axis. In such

Table 1
Mechanical properties of the PLA material (E: Youngs modulus; σ_y: yield stress; σ_u: ultimate tensile strength; υ: Poissońs ratio; L: critical distance).

E (MPa)	σ_y (MPa)	σ_u (MPa)	υ	L (mm)	K_{mat} (MPam$^{1/2}$)
2800 ± 400	35 ± 5	41 ± 6	0.29	0.20	4.9 ± 0.2

circumstances, K^N_{mat} is given by:

$$K^N_{mat} = K_{mat}\sqrt{1+\frac{\rho}{4L}} \quad (7)$$

The authors [11,17,18] proposed a methodology to assess notch-type defects using the BS7910 Option 1 FAD approach, which has been validated in metallic [11,19] and non-metallic materials [17,19], including additively manufactured PLA when testing SENB fracture specimens. The methodology assumes that both the FAL and the L_r parameter are not significantly affected by the notch tip: the L_r parameter depends on the limit load, whose variation with the notch radius is very limited [20], so the P_L solutions (or the σ_{ref} solutions) derived for cracked conditions may be used in notched conditions (i.e., L_r is the same as that used for cracks, equation (2), with available solutions in the literature for most of the practical situations); regarding the FAL solutions to be used in the analysis of notches, it is possible to use the FALs proposed in structural integrity assessment procedures for the analysis of crack-like defects, given that the dependence of such solutions on the notch radius is very weak, as shown in [21]. Alternatively, when analyzing different types of polyamide 12, Martínez et al. [16] have proposed the use of FALs derived from the consideration of the material specific tensile curve.

Consequently, the only notch correction required to use FADs in notch analysis is the one affecting K_r, which is defined as:

Table 2
Description of the experimental program, including geometrical parameters, experimental critical loads (P_{exp}), K_r and L_r coordinates, and resulting critical load estimations (P_{est}) derived from FAD analysis.

Defect	Specimen n°	a (mm)	W (mm)	ρ (mm)	B (mm)	P_{exp} (kN)	K_r	L_r	P_{est} (kN)	P_{est}/P_{exp}
U-notch	201	30.65	60.67	0.85	5.38	3.78	1.47	1.52	2.15	0.57
	202	30.63	60.66	0.94	4.88	3.97	1.66	1.76	2.00	0.50
	203	30.57	60.66	0.94	4.89	4.22	1.74	1.85	2.00	0.47
	204	30.16	60.81	0.89	10.22	9.06	1.76	1.82	4.20	0.46
	205	30.69	60.78	0.90	10.00	8.44	1.73	1.82	4.10	0.49
	206	30.77	60.78	0.89	10.01	8.86	1.83	1.92	4.10	0.46
	207	30.42	120.66	0.90	4.82	13.34	1.49	1.13	8.00	0.60
	208	30.69	120.56	0.89	4.92	12.52	1.39	1.05	8.00	0.64
	209	30.64	120.64	0.84	4.89	11.86	1.34	1.00	8.00	0.67
	210	30.50	120.38	0.93	9.98	23.52	1.26	0.97	16.50	0.70
	211	30.66	120.34	0.92	9.95	22.18	1.20	0.92	16.50	0.74
	212	30.67	120.38	0.94	9.97	24.26	1.31	1.00	16.50	0.68
	213	30.42	120.64	0.89	20.30	44.62	1.19	0.87	34.00	0.76
	214	30.42	120.64	0.89	20.30	43.62	1.16	0.85	34.00	0.78
	215	30.42	120.64	0.89	20.30	46.71	1.24	0.91	34.00	0.73
	301	30.63	60.70	1.32	4.82	3.92	1.49	1.75	2.10	0.53
	302	31.10	60.65	1.37	4.85	3.97	1.54	1.84	2.05	0.52
	303	30.74	60.64	1.29	4.94	3.96	1.50	1.75	2.10	0.53
	304	30.69	60.61	1.30	9.91	8.39	1.57	1.84	4.30	0.51
	305	30.57	60.62	1.33	9.86	7.55	1.40	1.65	4.30	0.57
	306	31.11	60.74	1.30	10.00	8.52	1.62	1.90	4.25	0.50
	307	30.76	120.54	1.31	4.83	12.80	1.30	1.09	8.70	0.68
	308	30.78	120.65	1.32	4.84	13.47	1.36	1.15	8.70	0.65
	309	30.85	120.74	1.31	4.93	12.23	1.21	1.02	8.80	0.72
	310	30.77	120.61	1.33	9.93	23.86	1.17	0.99	18.00	0.75
	311	31.11	120.40	1.31	9.84	24.36	1.23	1.03	17.50	0.72
	312	30.84	120.44	1.31	9.88	25.02	1.24	1.05	18.00	0.72
V-notch	401	26.95	60.72	1.14	4.84	3.37	1.04	1.13	2.65	0.79
	402	27.02	60.76	1.29	4.91	3.48	1.02	1.16	2.75	0.79
	403	27.16	60.87	1.58	4.9	3.45	0.96	1.15	2.85	0.83
	404	33.00	60.82	2.62	10.06	8.03	1.36	2.08	3.90	0.49
	405	32.94	60.61	3.43	9.93	8.32	1.29	2.20	3.90	0.47
	406	26.83	60.64	0.84	9.98	9.34	1.51	1.51	5.20	0.56
	407	26.81	120.63	1.05	4.89	11.09	1.04	0.85	9.50	0.86
	408	26.87	120.64	0.93	5.01	11.04	1.04	0.82	9.50	0.86
	409	26.82	120.60	1.04	4.75	11.06	1.07	0.87	9.00	0.81
	410	26.81	120.52	0.95	9.95	28.58	1.35	1.07	18.20	0.64
	411	26.68	120.48	0.93	9.99	30.09	1.42	1.12	18.20	0.60
	412	26.97	120.56	0.75	9.95	26.06	1.32	0.98	18.10	0.69
Hole	101	15.18	30.37	15.18	4.86	5.61	0.23	1.08	5.65	1.01
	102	15.12	30.40	15.12	4.91	5.42	0.21	1.02	5.75	1.06
	103	15.07	30.34	15.07	4.97	5.70	0.22	1.07	5.75	1.01
	104	15.13	30.39	15.13	10.09	12.63	0.24	1.16	11.80	0.93
	105	15.13	30.37	15.13	10.06	12.55	0.24	1.16	11.80	0.94
	106	Not valid								
	107	15.24	60.24	15.24	4.87	16.66	0.29	1.08	16.80	1.01
	108	15.13	60.24	15.13	4.95	17.56	0.31	1.11	16.90	0.96
	109	15.11	60.26	15.11	4.99	16.83	0.29	1.06	17.00	1.01
	110	15.03	60.24	15.03	10.31	34.02	0.28	1.03	35.50	1.04
	111	14.88	60.22	14.88	9.90	33.45	0.29	1.06	34.50	1.03
	112	14.81	60.21	14.81	9.99	33.56	0.29	1.05	35.00	1.04

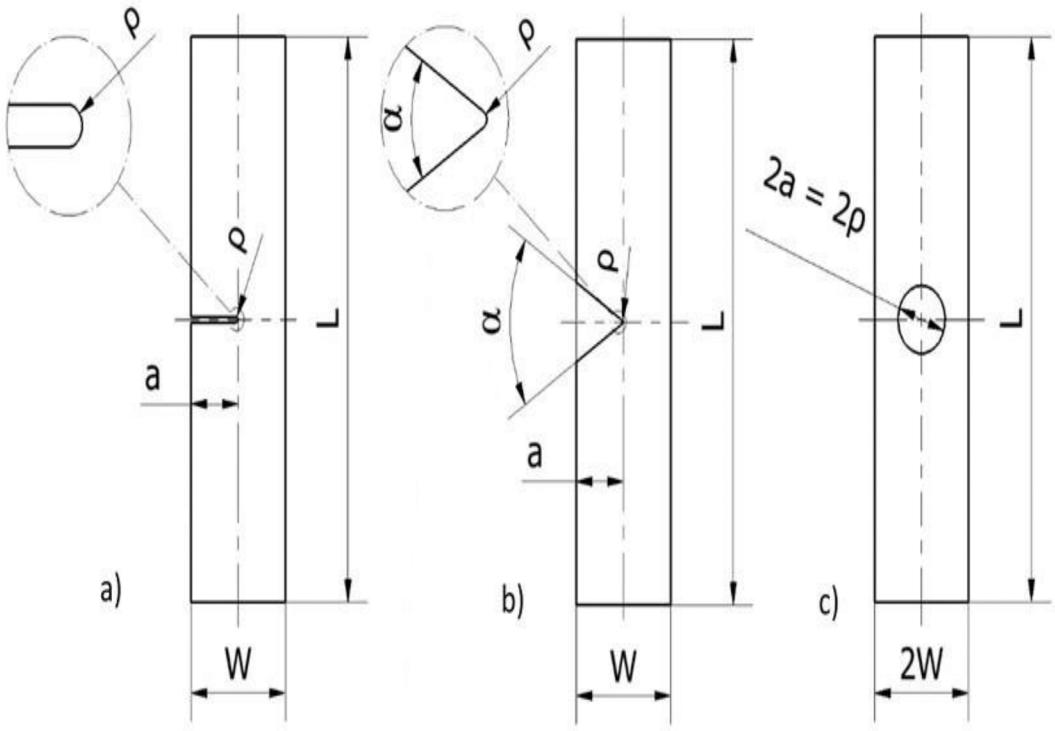

Fig. 3. Schematic of the tested specimens. a) U-notched specimens; b) V-notched specimens; c) specimens with central hole.

$$K_r = \frac{K_I}{K_{mat}^N} = \frac{K_I}{K_{mat}\sqrt{1+\frac{\rho}{4L}}} \tag{8}$$

Thus, the approach is actually substituting the real situation of a notched material whose fracture toughness is K_{mat}, with an equivalent situation of a cracked material whose fracture resistance is K_{mat}^N. In other words, the assessment of notches through Failure Assessment Diagrams only requires providing a correction of the material fracture resistance in the definition of the K_r parameter (e.g. equation (8)).

3. Materials and methods

The authors have published previous works [17,22] covering the analysis of the fracture behavior of this additively manufactured PLA material, using SENB specimens and covering three different raster orientations: 0/90, 30/-60 and 45/-45. However, this work will be focused on notched plates with just one raster orientation: 45/-45.

The previous works [17,22] are used here to define the basic tensile and fracture properties, together with the TCD parameters (L and σ_0). Here, suffice it to say that 3 tensile tests on dog-bone specimens and 20 fracture tests on SENB specimens (see Fig. 2) were performed. The fracture specimens covered five different notch radii: 0 mm, 0.25 mm, 0.50 mm, 1 mm and 2 mm (four tests per notch radius). The defects were machined, except for those whose notch radius was 0 mm (crack-like defects), which were produced by sawing using a razor blade. The experimental results obtained on the fracture specimens with different notch radii were also used to calibrate the material critical distance (L) [17] by simply performing the best fit (least squares) of the LM apparent fracture toughness equation (see equation (7)), with L being the fitting parameter.

All samples were manufactured by fused deposition modeling (FDM) with the following printing parameters: layer height 0.3 mm, nozzle diameter 0.4 mm, infill level 100%, printing temperature 200 °C, bed temperature 75 °C, and printing rate 30 mm/s. Again, additional details may be found in [22].

Tensile tests were performed at room temperature following ASTM D638 [23], whereas fracture tests were performed at room temperature following ASTM D6068 [24] standard. The results of this initial characterization program (average values and standard deviations) are shown in Table 1, with the full details being gathered in [17,22]. Here, it is important to note the authors have previously shown [17] that the use of fracture toughness results derived from ASTM D6068 may generate non-conservative FAD analyses in additively manufactured polymers, although for this particular material (PLA) and raster orientation (45/−45), the ASTM D6068 standard provided more accurate results than its linear-elastic counterpart (ASTM 5045 [25]).

In order to complete the present research, and once the basic material mechanical behavior is known, this material was used to generate 51 plates combining 3 types of notches (U-notches V-notches and holes), widths (W), thicknesses (B) and notch length to width ratios (a/W). The whole experimental program is described in Table 2, with Fig. 3 showing a schematic of the tested plates and Fig. 4 showing one of the specimens before being tested. All of them were printed with the same printing parameters used for the tensile and SENB fracture specimens (described above). The real (measured) values of the geometrical parameters of the notches are included, as they were substantially different from the initially (nominal) ones. The results shown in section 4 were obtained with these real values.

The loading rate was 1 mm/min in all cases (same rate used in [22] for tensile and fracture characterization), and the load–displacement curve was recorded for each individual test, also determining the corresponding critical (i.e., maximum) loads, which are also shown in Table 2. Fig. 5 shows examples of the obtained load–displacement curves, revealing the effect of the different parameters covered by the experimental program (i.e., thickness, a/W ratio, notch radius, type of defect, etc.).

Here, it is important to note that equation (8) is derived from the Creager-Paris stress solution for U-notches, which are in principle more severe defects than V notches or holes with the same notch radius. The FAD approach used here, therefore, would be initially indicated for the U-notched plates included in the experimental program. However, Lazzarin and Berto showed [26] how V-notches with opening angles

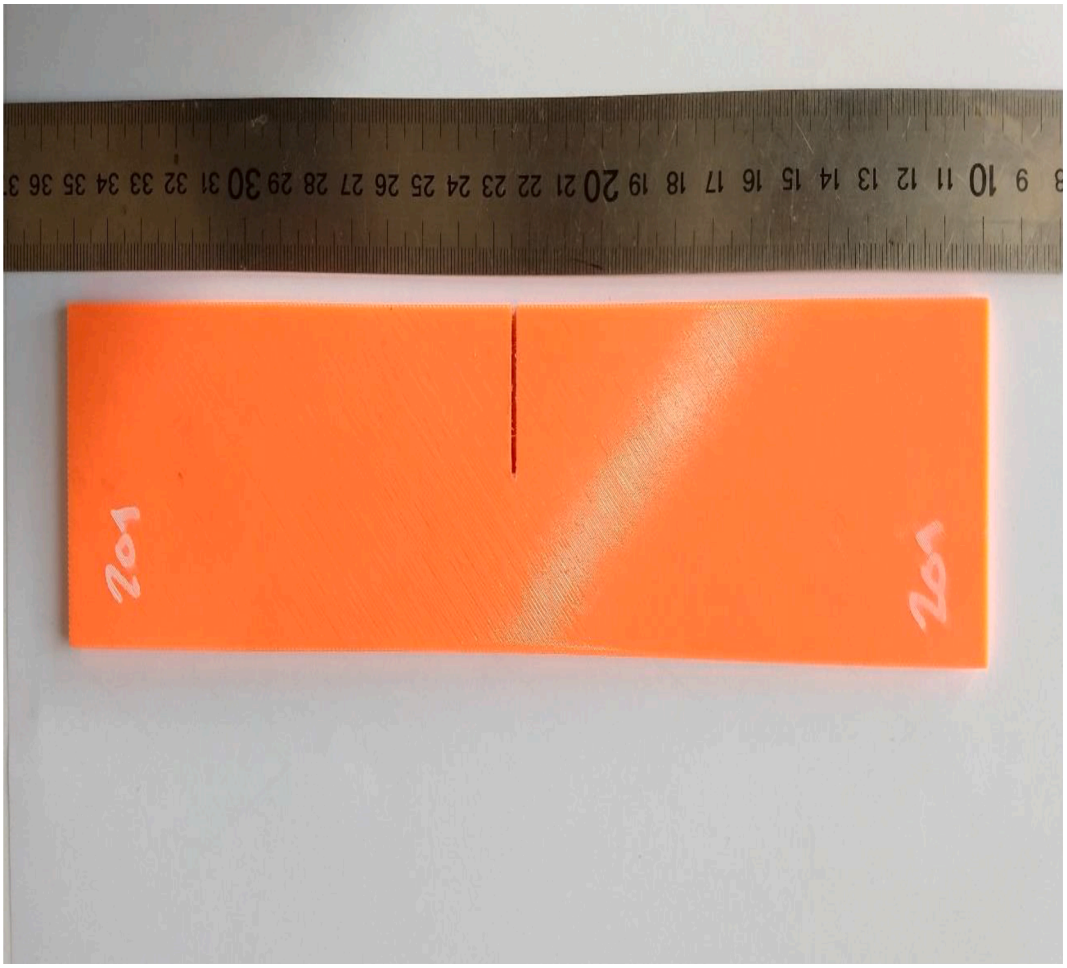

Fig. 4. Tested specimen (n° 201), with a/W = 0.5, W = 60 mm, ρ = 0.9 mm and B = 5 mm (nominal values).

(2α) below 90° provided similar critical loads to those of U-notches (2α = 0°) in PMMA material. Thus, the authors decided to include V-notches with 2α = 60° to check the accuracy of the approach under such conditions and, as an additional particular geometrical condition, specimens containing holes.

Additionally, provided that the tensile specimens, the fracture characterization specimens and the notched plates have the same raster orientation, that all the involved defects (crack-like defects and notches in fracture SENB specimens and notched plates) are identically oriented regarding such raster orientation, and also that the different specimens are all printed flat on the build plate (as it is the case here), the material can be modelled as a homogenous and isotropic material. This was justified and validated in [27], with additional experimental evidence in [17,22].

After testing, the FAD approach, including the notch correction provided by equation (8), was applied to analyze its suitability for evaluating the fracture behavior of additively manufactured PLA notched specimens. BS7910 Option 1 FAL was used in all cases whereas K_I solutions and P_L solutions were taken from [28]. Summarizing, the analytical process is as follows:

- Define FAL, using BS7910 equations for Option 1 (equations (9) to (14)):

$$K_r = f(L_r) = \left[1 + \frac{1}{2}(L_r)^2\right]^{-1/2} \bullet \left[0.3 + 0.7 \bullet e^{-\mu \bullet (L_r)^6}\right] L_r \leq 1 \tag{9}$$

$$K_r = f(L_r) = f(1) \bullet L_r^{\frac{N-1}{2N}} 1 < L_r \leq L_{r,max} \tag{10}$$

$$K_r = f(L_r) = 0 L_r = L_{r,max} \tag{11}$$

$$\mu = min\left[0.001 \bullet \frac{E}{\sigma_y}; 0.6\right] \tag{12}$$

$$N = 0.3 \bullet \left(1 - \frac{\sigma_y}{\sigma_u}\right) \tag{13}$$

$$L_{r,max} = \frac{\sigma_y + \sigma_u}{2 \bullet \sigma_y} \tag{14}$$

The use of equations (12) and (13) to define μ and N in non-metallic materials has been previously validated by the authors in [15] for polymers, composites and rocks, and in [17] for additively manufactured polymers and composites. The values of E, σ_y and σ_u are taken from Table 1.

- Define L_r using equation (2), as it is done for crack-like defects, with the P_L solutions provided by [14] for edge cracks (in the case of U- and V-notches) and through thickness cracks (in the case of holes) in finite plates. The value of P used to define L_r is the corresponding experimental critical load (P_{exp}, see Table 2). Additionally, it should be noted that three of the notched plates (n° 213,214 and 215: U-notched plates with nominal B = 20 mm) were in an intermediate situation between plane stress and plane strain conditions, so for these cases, the P_L values used in the assessment were actually derived from the linear interpolation between the plane stress and plane strain solutions of P_L provided in [14]. Interpolation limits were given by equations (15) and (16) for plane strain and plane stress conditions, respectively [5], with the K^N_{mat}

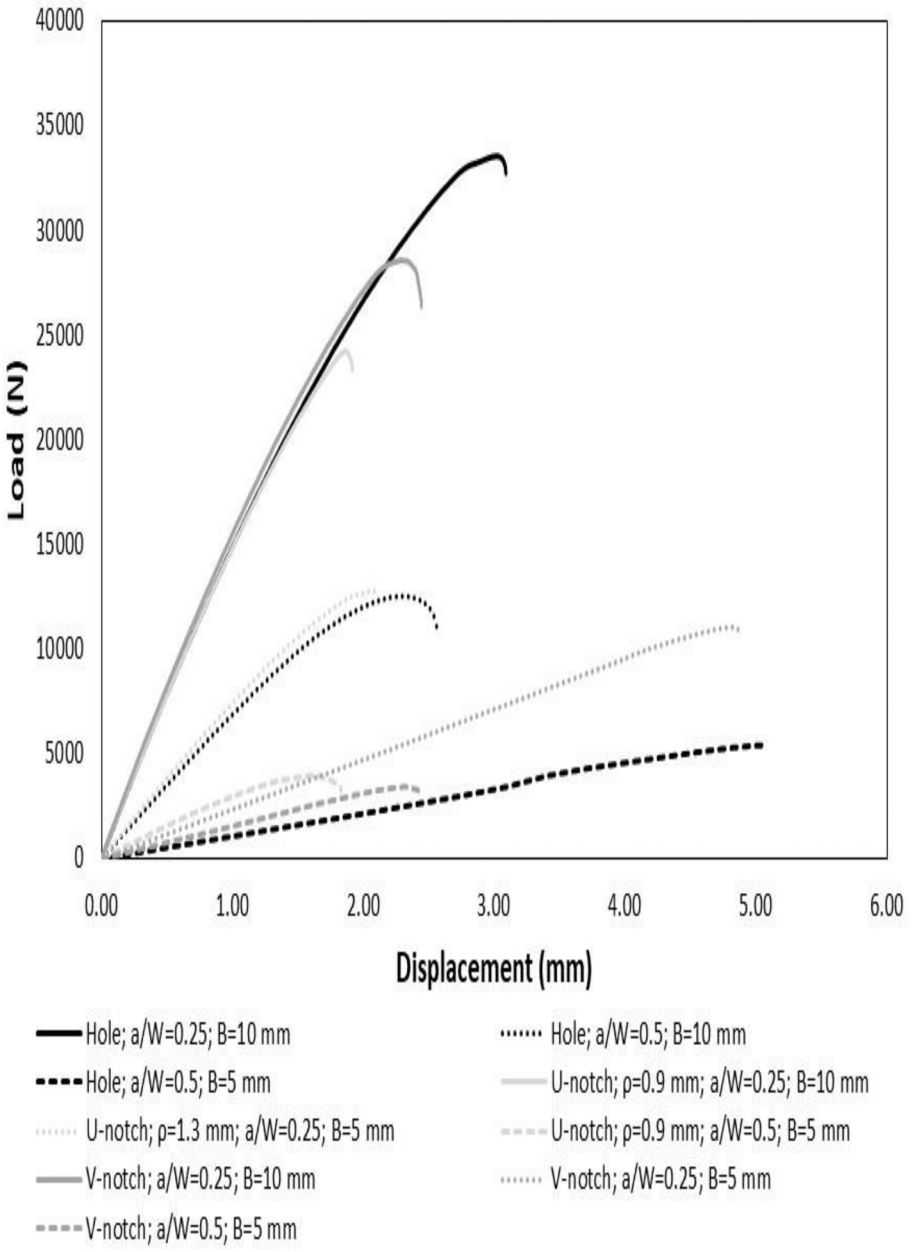

Fig. 5. Examples of the load–displacement curves developed by the (tensile) tested notched plates.

values derived from equation (7) and B being the plate thickness. Thus, when equation (15) is met (none of the specimens in the present work), the plane strain solution for P_L is used; when equation (16) is fulfilled (most of the specimens analyzed here), the plane stress solution is used; for intermediate situations (specimens n° 213, 214 and 215), the mentioned interpolation is performed:

$$B \geq 2.5\left(\frac{K^N_{mat}}{\sigma_y}\right)^2 \tag{15}$$

$$B \leq \frac{1}{\pi}\left(\frac{K^N_{mat}}{\sigma_y}\right)^2 \tag{16}$$

The different P_L solutions are given by equations (17) and (18) for U-notched and V-notched plates (P_L solutions provided in [14] for edge cracked tension plates), and equations (19) and (20) for plates with central hole (P_L solutions provided in [14] for middle tension plates):

$$P_L = 1.445\hat{A}\cdot\left(\sqrt{1+\left(\frac{a}{b}\right)^2}-\frac{a}{b}\right)\hat{A}\cdot B\hat{A}\cdot b\hat{A}\cdot\sigma_y(\text{plane strain}) \tag{17}$$

$$P_L = 1.072\hat{A}\cdot\left(\sqrt{1+\left(\frac{a}{b}\right)^2}-\frac{a}{b}\right)\hat{A}\cdot B\hat{A}\cdot b\hat{A}\cdot\sigma_y \text{ (plane stress)} \tag{18}$$

$$P_L = \frac{2}{\sqrt{3}}\hat{A}\cdot B\hat{A}\cdot b\hat{A}\cdot\sigma_y(\text{plane strain}) \tag{19}$$

$$P_L = 2\hat{A}\cdot B\hat{A}\cdot b\hat{A}\cdot\sigma_y(\text{plane stress}) \tag{20}$$

a is the defect length, b is the remaining ligament (W-a), B is the plate thickness, and σ_y is the material yield stress.

- Define K_r, with the K_I solutions provided by [28] for edge cracks in finite plates in case of U-notch and V-notch analyses, and for through thickness cracks in finite plates in the case of holes. K_I values are also

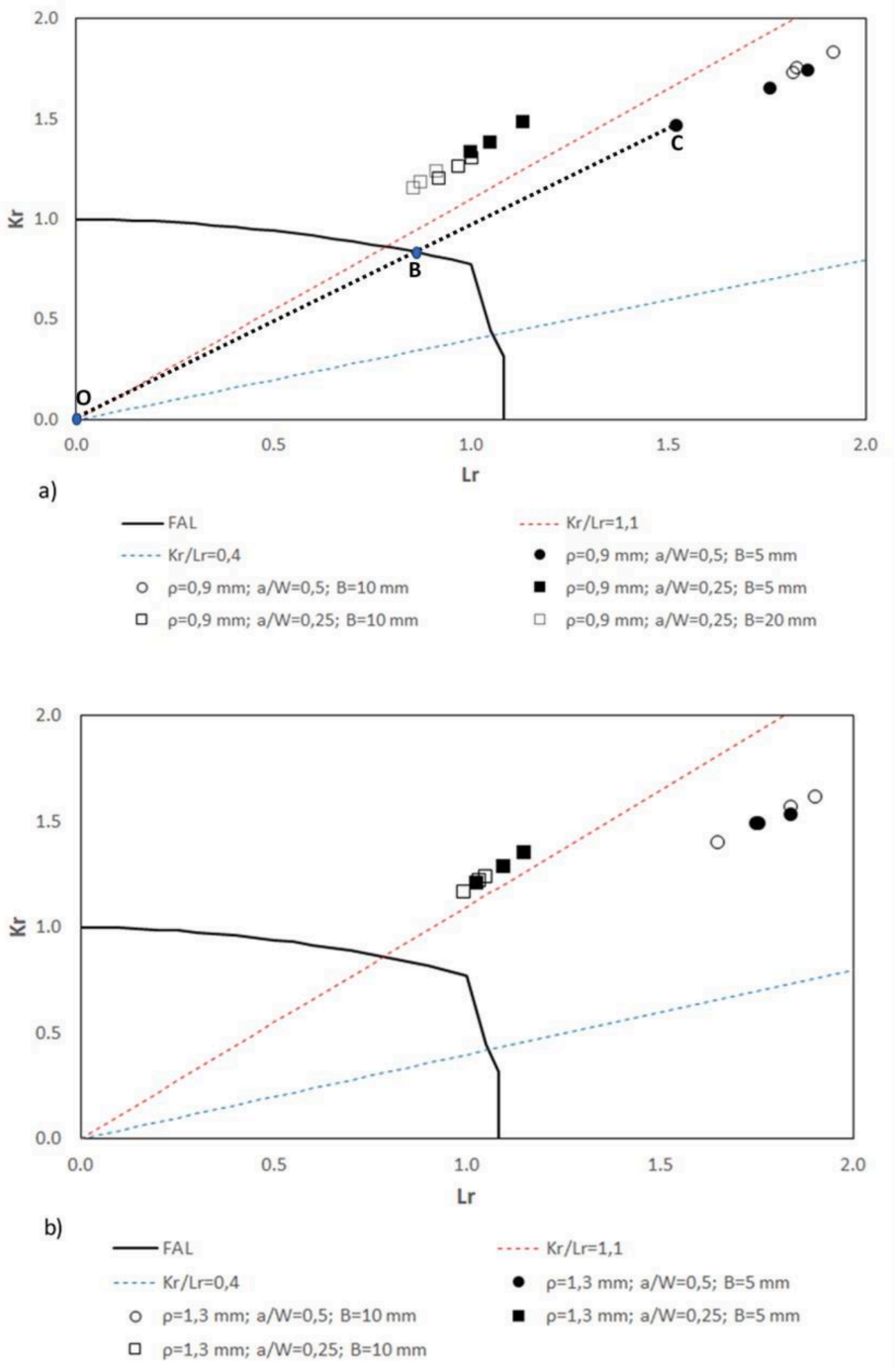

Fig. 6. FAD assessment of the U-notched tested plates, and definition of the calculation of the corresponding critical loads. Geometrical parameters refer to nominal values. a) specimens n° 201 to n° 215; b) specimens n° 301 to n° 312.

calculated, again and for each specimen, for the corresponding experimental critical load. Finally, K^{N}_{mat} is calculated following equation (8) for the notch radius (ρ) being analyzed, and using the K_{mat} and L values shown in Table 1. Thus, this third step is the one introducing the notch correction in the analysis.

- Represent the (K_r, L_r) coordinates of each specimen in the FAD. As long as they correspond to a critical situation, if the FAD analysis of the notched specimens is safe (i.e., provides conservative results), the assessment points should be located above the FAL. On the contrary, if the assessment points at failure lie within the area below the FAL, the FAD would be assessing a critical situation as safe.

4. Results and discussion

Table 2 gathers the obtained estimation of the critical load (P_{est}) for each one of the tested specimens, as well as the ratio between the critical load estimation and the experimental critical load (P_{est}/P_{exp}). Figs. 6–8 show the resulting FAD with all the assessment points.

It can be easily observed that all the assessment points for U-notches (Fig. 6) and V-notches (Fig. 7) are located above the FAL, meaning that the assessment points at failure are located in the unsafe area. The critical loads shown in Table 2 are calculated as shown in Fig. 6a: for a given specimen, the critical load corresponds to that one providing an assessment point that it is exactly located on the FAL (point B). Thus,

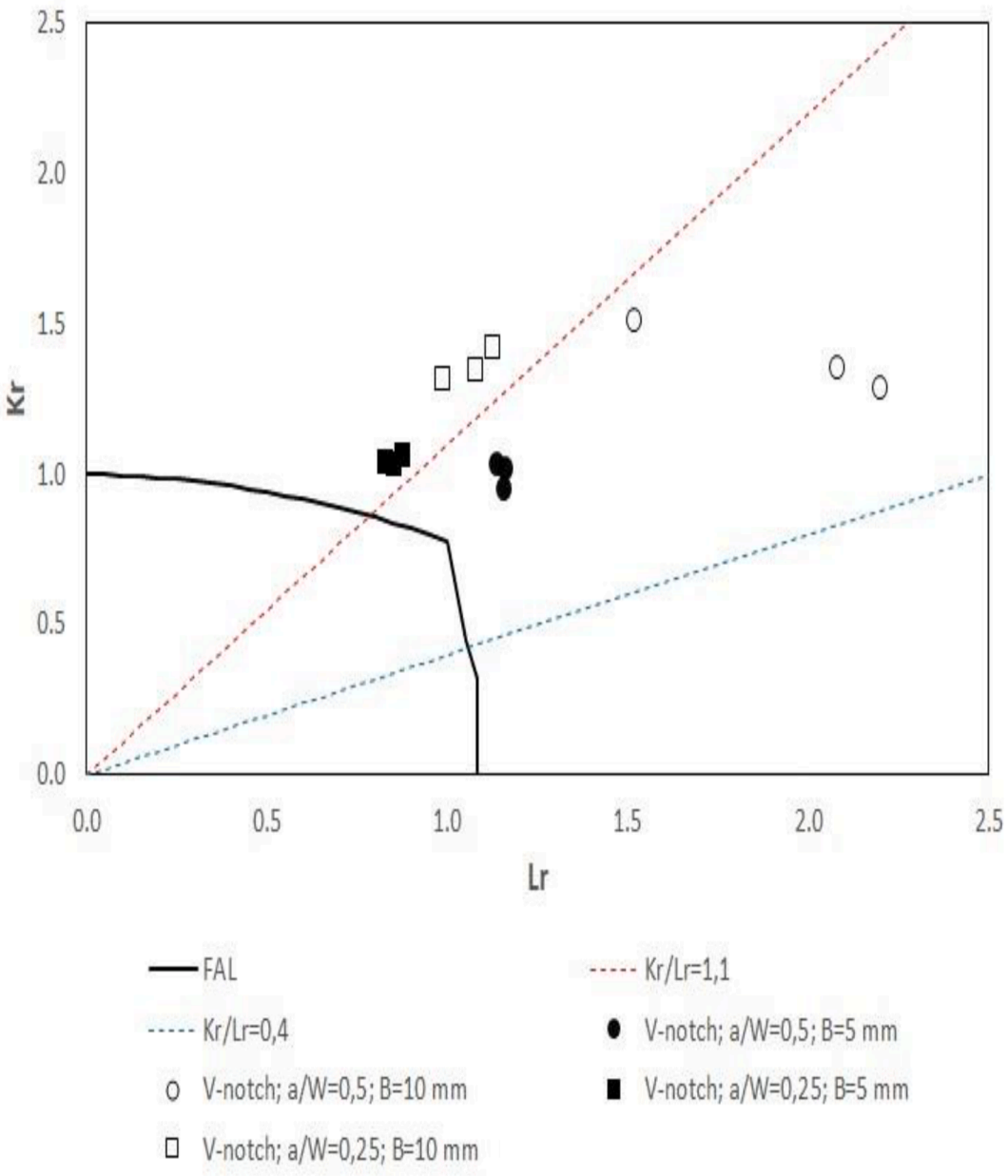

Fig. 7. FAD assessment of the V-notched tested plates. Geometrical parameters refer to nominal values. Specimens n° 401 to n° 412.

given that the defect length (a) is constant and the *iso*-a lines are straight lines, the critical load is directly obtained from equation (21):

$$P_{est} = P_{exp}\hat{A}\cdot\frac{\overline{OB}}{\overline{OC}} \quad (21)$$

The proposed approach, therefore, provides safe estimations of the critical loads for U-notched and V-notched specimens, with a significant amount of conservatism. The main source of the conservatism may be caused by the low level of constraint of the loaded plates, which are tested under tensile conditions, if compared with the high conservatism of the SENB specimens used to determine the material fracture toughness and the notch effect [22]. The effect of low constraint in fracture assessments, and the corresponding conservatism of the fracture analyses, has been widely analyzed in metallic materials, with abundant literature and open issues still requiring further research [29–32]. The scope of this work is not focused on low constraint analysis in additively manufactured polymers, so here, suffice it to say that the conservatism obtained here is comparable (i.e., very similar) to that obtained when assessing, using FADs without any constraint correction, metallic plates subjected to tensile loads [29–32].

Moreover, the assessment points are located above the $K_r/L_r = 1.1$ (slope) line, suggesting that fracture dominates the failure of the plates [1], or between the slopes 0.4 and 1.1, suggesting that elastic–plastic conditions control such process [1].

Regarding the results for the different geometrical conditions, the conservatism observed in U-notches is slightly larger than that obtained in V-notches, with average P_{est}/P_{exp} ratios of 0.61 and 0.70, respectively. This agrees with the fact that here, it has been assumed that V-notches and holes behave similarly. The difference between U-notches and V-notches ($2\alpha = 60°$) is, in any case, very small, in agreement with [26].

Within the U-notches, the conservatism is totally analogous for plates with nominal notch radii of 0.90 and 1.30 mm, and it is higher for (nominal) a/W = 0.5 than for a/W = 0.25, with no significant differences between the results obtained with different thicknesses. However, in V-notched plates, the conservatism observed in thicker specimens (nominal thickness, B = 10 mm) is significantly higher than that

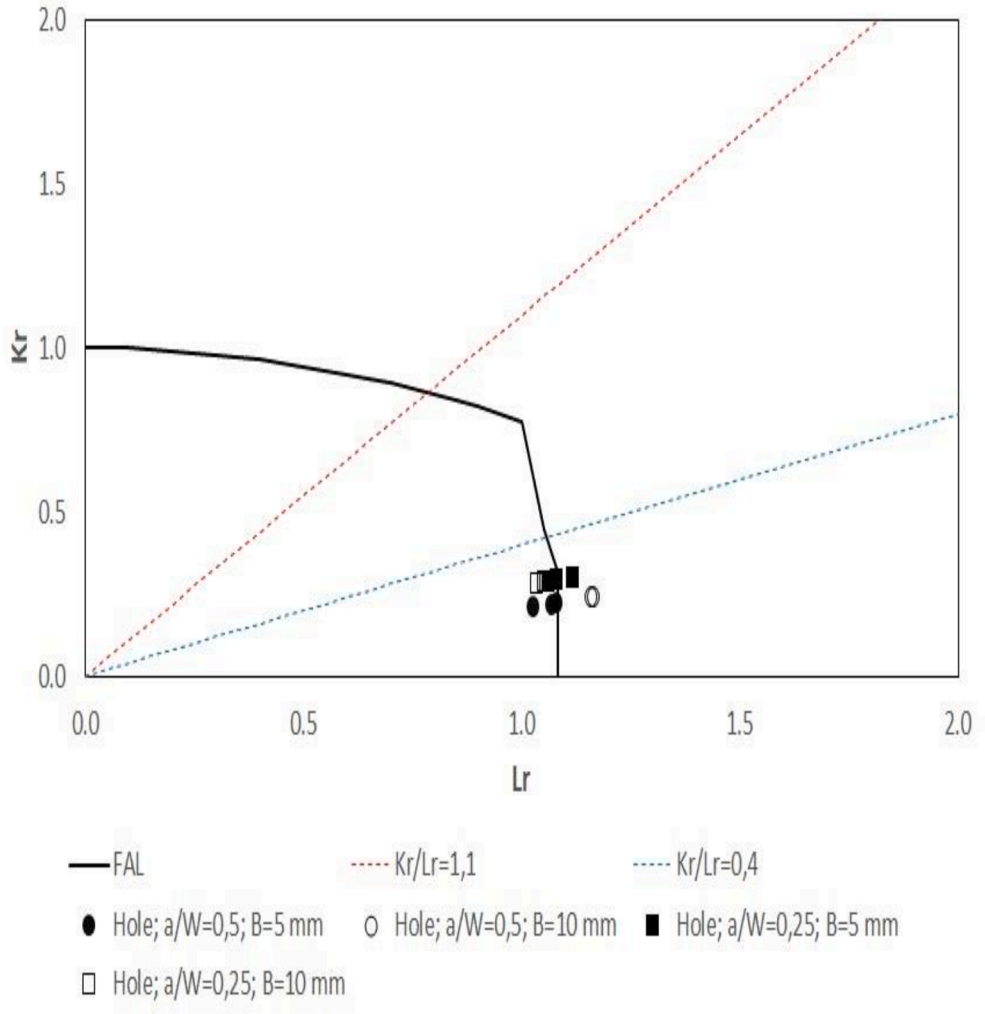

Fig. 8. FAD assessment of the tested plates with central hole. Geometrical parameters refer to nominal values. Specimens n° 101 to n° 112.

observed in thinner plates (B = 5 mm).

Finally, the results of the assessment for plates with a central hole are significantly different. In this case, the accuracy is surprising considering that the holes have been assessed as U-notches, and also that the Creager-Paris stress distribution was defined for slender U-notches, far from the situation represented by the holes. The predictions range within ±6% of the experimental critical loads. However, many of the predictions tends to be slightly unsafe, with P_{est}/P_{exp} ratios above 1.0. When trying to justify these results, it is important to note that the assessment points are located below the $K_r/L_r = 0.4$ slope, suggesting plastic collapse dominated failures [1]. This agrees with the load–displacement curves obtained in these plates, which tend to develop a higher level of non-linearity that that developed in U-notched and V-notched plates (see Fig. 5). Thus, the reasons of the unsafe predictions could be partially found in the proper plastic collapse analysis. Additionally, it is important to note that the definition of K_r uses K^N_{mat} solutions derived from the Creager-Paris stress distribution [18], which is valid for slender U-notches and, therefore, is being applied beyond its validity range when analyzing holes. Thus, the conservatism observed in the U-notched and V-notched plates may be being compensated by the use of unsafe K^N_{mat} estimations when analyzing hole-type defects, providing by chance in this research the observed accuracy. Further research is needed in this sense, but from the results obtained here it can be suggested that plastic collapse (or limit load) solutions used in traditional materials (e.g., metals) may be unsafe for additively manufactured materials with numerous internal defects, as it is the case of the PLA material analyzed in this research, and also (or) that the use of K^N_{mat} estimations derived from the Creager-Paris stress solution may be unsafe for holes.

Here, it is worth mentioning that the analyses performed in this work have used average experimental values of tensile and fracture properties, with the aim of analyzing the capacity of the FAD approach to assess the physical process of fracture/plastic collapse. However, when using structural integrity procedures (e.g., [3,4]), the material properties used in the assessments are typically lower bound values obtained through (generally) simple statistical rules. This sums additional conservatism to the analysis.

To conclude with the discussion, some analysis of the cracking behavior was performed. Analogously to the findings of Tse Ng and Susmel [27], in the presence of the different types of notches analyzed here, cracks initiated at the corresponding notch tip. In this case, however, cracking took place on material planes that were not always macroscopically perpendicular to the loading direction, and resulted from a combination of different micromechanisms (debonding between adjacent/printing layers, debonding of filaments and cracking of the filaments). The specific micromechanisms observed in the different specimens were as follows:

- U-notched and V-notched plates behaved similarly. In both cases, thinner specimens (nominal B = 5 mm) developed, after the peak load, clear macroscopic cracking planes oriented at +45° (or −45°) that resulted from a combination of the debonding of the filaments oriented at +45° (or −45°) and the failure of filaments oriented at −45° (or

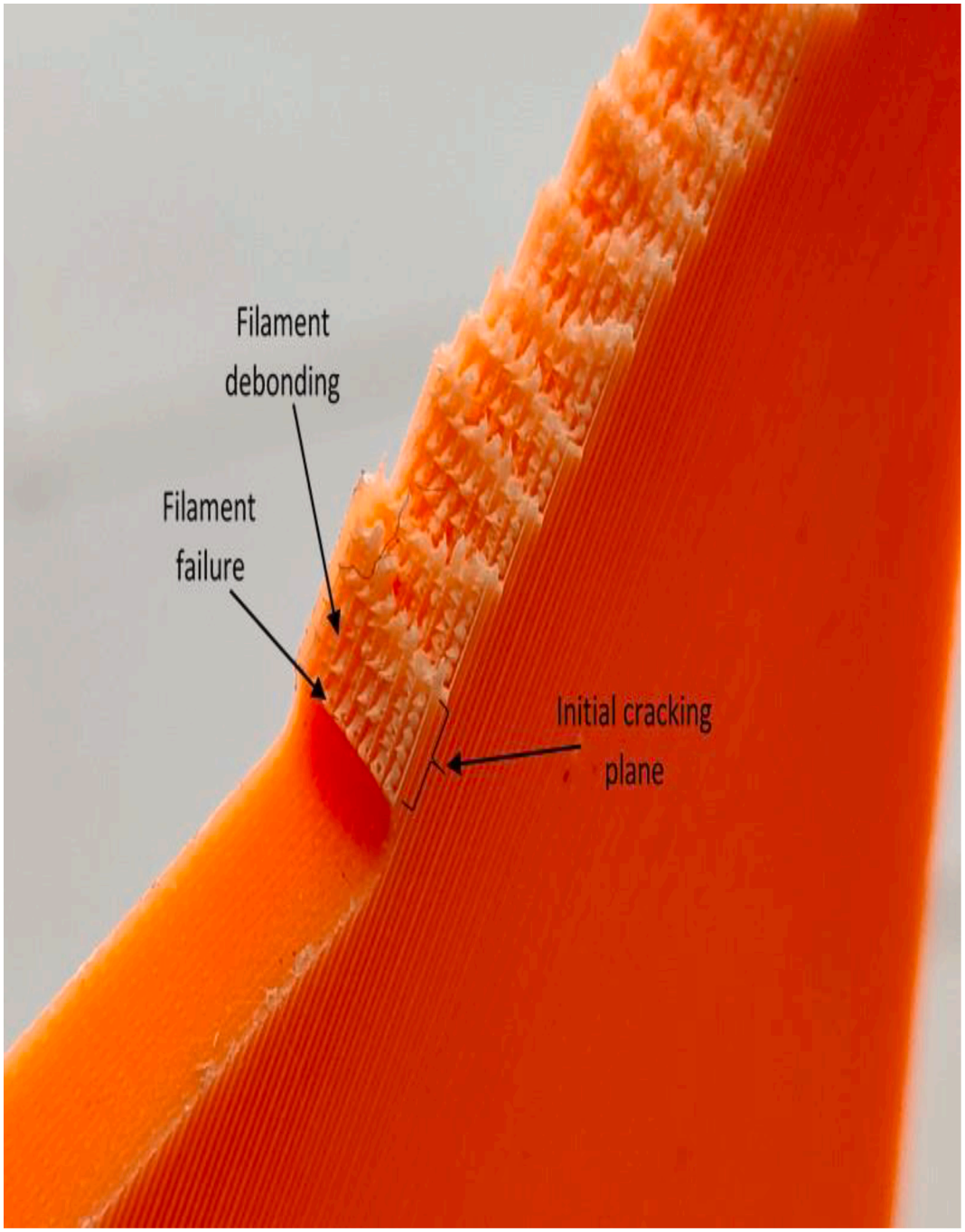

Fig. 9. Macrograph of the cracking behavior of specimen n° 302 (nominal values of B and W are 5 mm and 60 mm, respectively).

+45°). The initial plane was generally followed by a zig-zag pattern with a dominant orientation at −45° (or +45°), as shown in Fig. 9. On the contrary, thicker specimens (nominal B = 10–20 mm), showed from the initiation of the cracking path the mentioned zig-zag behavior that resulted from a succession of much smaller planes alternatively oriented at + 45° and −45° and caused by the above-mentioned combination of mechanisms. In both cases, the wider specimens (nominal W = 120 mm) also developed debonding between printing layers at the end of the cracking process. Figs. 9 and 10 show some examples of the observed behavior.

- The plates with central hole presented similar behavior for the two values of thickness analyzed in this work (5 mm and 10 mm) and the two values of nominal (half) width (30 mm and 60 mm). The cracking behavior is a very complex process resulting from a combination of filament failures, debonding between filaments and debonding between printing layers. Fig. 11 shows an example of these fracture surfaces.

5. Conclusions

This paper proposes an approach for the assessment of additively manufactured plates containing notches. The approach is based on the joint application of the Failure Assessment Diagram (FAD) methodology and the notch correction derived from the Theory of Critical Distances (TCD). The latter is, additionally, based on the Creager-Paris stress distribution, so in principle, it only addresses the analysis of U-notches.

The approach has been validated through its application to an experimental program composed of 51 plates that combine different types of notches (U-notches, V-notches and circular holes) thicknesses

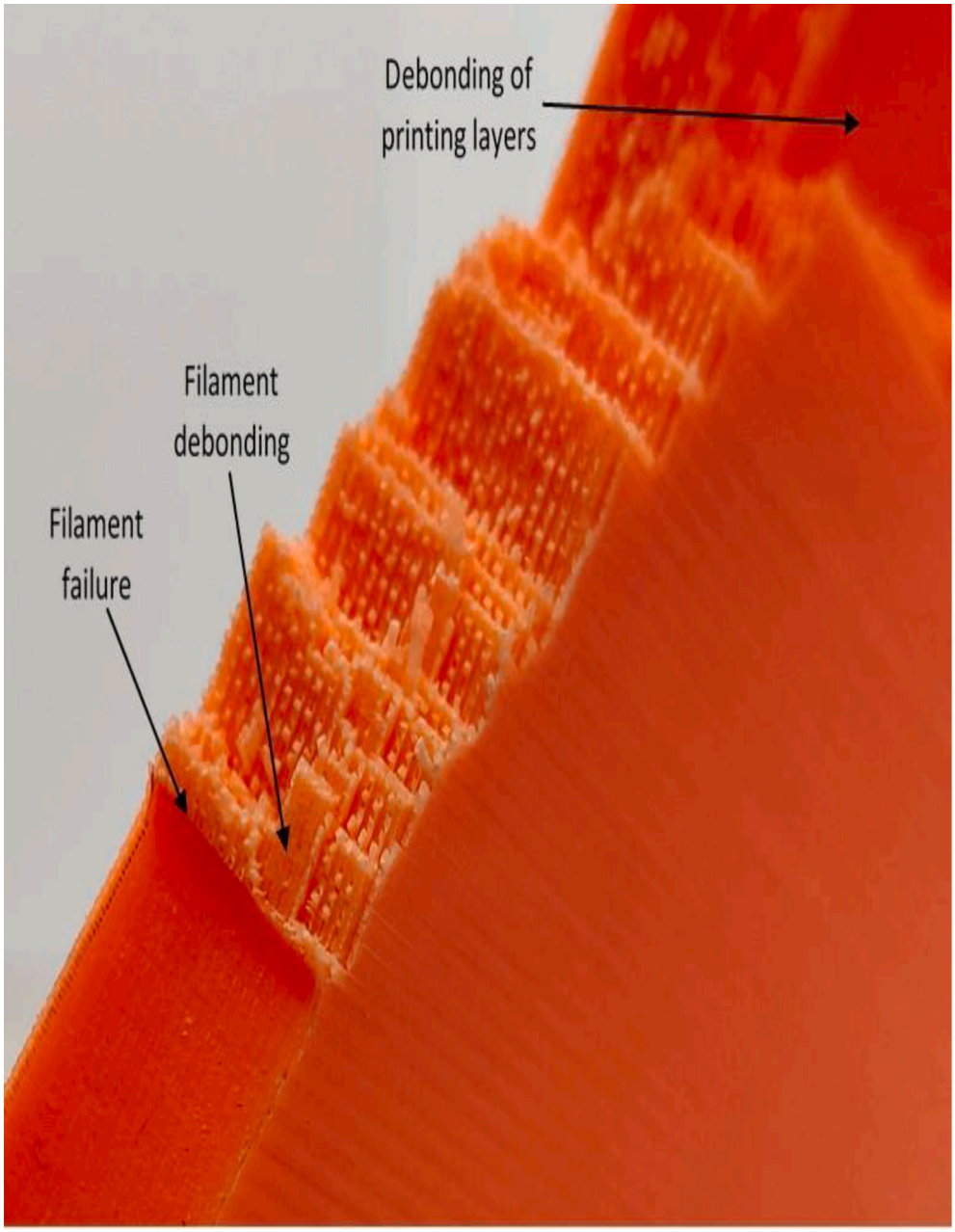

Fig. 10. Macrograph of the cracking behavior of specimen n° 410 (nominal values of B and W are 10 mm and 120 mm, respectively).

(5 mm to 20 mm), notch length to plate width ratios, and notch radii. V-notches and circular holes, which generate less demanding stress fields than U-notches, have been conservatively assumed to behave as U-notches.

The results obtained in this work demonstrate that the proposed approach may be used to generate safe conservative estimations of critical loads in U-notched and V-notched plates. The conservatism obtained in the results may have been caused by the low constraint conditions derived from the tensile loads applied to the plates, specially when compared to the high constraint conditions of the SENB specimens used for the characterization of the material fracture toughness. This conservatism, in any case, is comparable to that reported in the literature, and accepted in practice, for metallic materials subjected to low constraint conditions.

In the case of plats with central hole, the analysis has provided more accurate slightly unsafe predictions of the critical loads, and has predicted plastic-collapse dominated failures. This suggests that conventional solutions of limit loads should be used with caution in this kind of additively manufactured polymeric materials.

The cracking behavior was not the same in the different specimens, although in all cases the fracture process resulted from a complex combination of different micromechanisms, including debonding between filaments, debonding between printing layers and filament failures.

CRediT authorship contribution statement

Sergio Cicero: Conceptualization, Investigation, Methodology, Writing – original draft, Funding acquisition. **Sergio Arrieta:** Investigation, Data curation, Writing – review & editing. **Marcos Sánchez:** Investigation, Data curation, Writing – review & editing. **Laura Castanon-Jano:** Resources, Investigation.

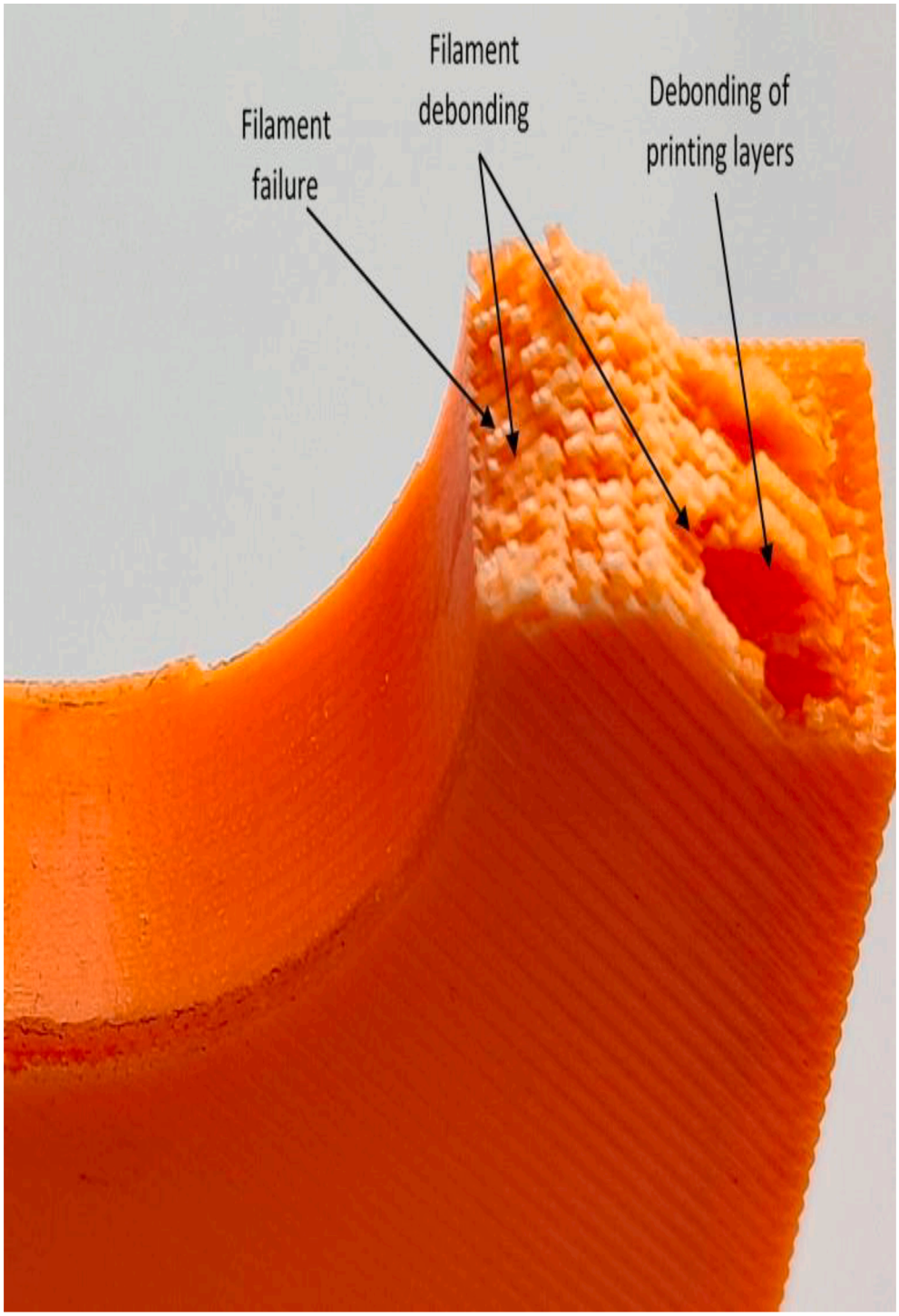

Fig. 11. Macrograph of the cracking behavior of specimen n°104 (nominal values of B and 2 W are 10 mm and 60 mm respectively).

Declaration of Competing Interest

The authors declare that they have no known competing financial interests or personal relationships that could have appeared to influence the work reported in this paper.

Data availability

Data will be made available on request.

Acknowledgements

This publication is part of the project "Comportamiento en fractura y efecto entalla en compuestos de matriz termoplástica obtenidos por fabricación aditiva, PID2021-122324NB-I00" funded by MCIN/ AEI /10.13039/501100011033/FEDER "Una manera de hacer Europa".

References

[1] M. Kocak, S. Webster, J.J. Janosch, R.A. Ainsworth, R. Koers, FITNET fitness-for-service (FFS) Procedure, Vol. 1, GKSS Hamburg, Germany, 2008.

[2] F. Gutiérrez-Solana, S. Cicero, FITNET FFS procedure: a unified European procedure for structural integrity assessment, Eng. Fail. Anal. 16 (2009) 559–577, https://doi.org/10.1016/j.engfailanal.2008.02.007.
[3] BS 7910:2019, Guide to methods for assessing the acceptability of flaws in metallic structures, British Standard Institution, London, UK, 2019.
[4] API RP 579-1 / ASME FFS-1, API 579-1/ASME FFS-1, Third edition, The American Society of Mechanical Engineers, New York, USA, 2016.
[5] D. Taylor, The theory of critical distances: a new perspective in fracture mechanics, Elsevier, UK, 2007.
[6] S. Cicero, V. Madrazo, I.A. Carrascal, Analysis of notch effect in PMMA by using the theory of critical distances, Eng. Fract. Mech. 86 (2012) 56–72, https://doi.org/10.1016/j.engfracmech.2012.02.015.
[7] V. Madrazo, S. Cicero, I.A. Carrascal, On the point method and the line method notch effect predictions in Al7075-T651, Eng. Fract. Mech. 79 (2012) 363–379, https://doi.org/10.1016/j.engfracmech.2011.11.017.
[8] S. Cicero, V. Madrazo, T. García, J. Cuervo, E. Ruiz, On the notch effect in load bearing capacity, apparent fracture toughness and fracture mechanisms of polymer PMMA, aluminium alloy Al7075-T651 and structural steels S275JR and S355J2, Eng. Fail. Anal. 29 (2013) 108–121, https://doi.org/10.1016/j.engfailanal.2012.11.010.
[9] S. Cicero, V. Madrazo, T. García, Analysis of notch effect in the apparent fracture toughness and the fracture micromechanisms of ferritic-pearlitic steels operating within their lower shelf, Eng. Fail. Anal. 36 (2014) 322–342, https://doi.org/10.1016/j.engfailanal.2013.10.021.
[10] S. Cicero, F. Gutierrez-Solana, A.J. Horn, Experimental analysis of differences in mechanical behaviour of cracked and notched specimens in a ferritic-pearlitic steel: considerations about the notch effect on structural integrity, Eng. Fail. Anal. 16 (2009) 2450–2466, https://doi.org/10.1016/j.engfailanal.2009.04.003.
[11] S. Cicero, V. Madrazo, I.A. Carrascal, R. Cicero, Assessment of notched structural components using failure assessment diagrams and the theory of critical distances, Eng. Fract. Mech. 78 (2011) 2809–2825, https://doi.org/10.1016/j.engfracmech.2011.08.009.
[12] A. Hilleborg, M. Modeer, P.E. Petersson, Analysis of crack formation and crack growth in concrete by means of fracture mechanics and finite elements, Cem. Concr. Res. 6 (1976) 773–781, https://doi.org/10.1016/0008-8846(76)90007-7.
[13] W. Weibull, The phenomenon of rupture in solids, Proc. R. Swed. Inst. Eng. Res. 153 (1939) 1–55.
[14] G.C. Sih, Strain-energy-density factor applied to mixed mode crack problems, Int. J. Fract. 10 (1974) 305–321, https://doi.org/10.1007/BF00035493.
[15] J.D. Fuentes, S. Cicero, F.T. Ibáñez-Gutiérrez, I. Procopio, On the use of British standard 7910 option 1 failure assessment diagram to non-metallic materials, Fatigue Fract. Eng. Mater. Struct. 41 (2018) 146–158, https://doi.org/10.1111/ffe.12668.
[16] M. Martínez, A.J. Cano, A. Salazar, J. Rodríguez, On the failure assessment diagram methodology in polyamide 12, Eng. Fract. Mech. 269 (2022), 108558, https://doi.org/10.1016/j.engfracmech.2022.108558.
[17] S. Cicero, M. Sanchez, V. Martínez-Mata, S. Arrieta, B. Arroyo, Structural integrity assessment of additively manufactured ABS, PLA and graphene reinforced PLA notched specimens combining failure assessment diagrams and the theory of critical distances, Theor. Appl. Fract. Mech. 121 (2022), 103535, https://doi.org/10.1016/j.tafmec.2022.103535.
[18] M. Creager, P.C. Paris, Elastic field equations for blunt cracks with reference to stress corrosion cracking, Int. J. Fract. Mech. 3 (1967) 247–252, https://doi.org/10.1007/BF00182890.
[19] S. Cicero, V. Madrazo, García, T, on the assessment of U-shaped notches using failure assessment diagrams and the line method: experimental overview and validation, Theor. Appl. Fract. Mech. 80 (2015) 235–241, https://doi.org/10.1016/j.tafmec.2015.07.002.
[20] A.G. Miller, Review of limit loads of structures containing defects, Int. J. Press. Vessel Pip. 32 (1988) 197–327, https://doi.org/10.1016/0308-0161(88)90073-7.
[21] A.J. Horn, A.H. Sherry, An engineering assessment methodology for non-sharp defects in steel structures - Part I: procedure development, Int. J. Press. Vessel. Pip. 89 (2012) 137–150, https://doi.org/10.1016/j.ijpvp.2011.10.014.
[22] S. Cicero, V. Martínez-Mata, L. Castanon-Jano, A. Alonso-Estebanez, B. Arroyo, Analysis of notch effect in the fracture behaviour of additively manufactured PLA and graphene reinforced PLA, Theor. Appl. Fract. Mech. 114 (2021), 103032, https://doi.org/10.1016/j.tafmec.2021.103032.
[23] ASTM D638-14, Standard Test Method for Tensile Properties of Plastics, ASTM International West Conshohocken, PA, 2014.
[24] ASTM D6068-10(2018), Standard Test Method for Determining J-R Curves of Plastic Materials, ASTM International, West Conshohocken, PA, 2018.
[25] ASTM D5045-14, Standard Test Methods for Plane-Strain Fracture Toughness and Strain Energy Release Rate of Plastic Materials, ASTM International, West Conshohocken, PA, 2014.
[26] P. Lazzarin, F. Berto, Some expressions for the strain energy in a finite volume surrounding the root of blunt V-notches, Int. J. Fract. 135 (2005) 161–185, https://doi.org/10.1007/s10704-005-3943-6.
[27] C.T. Ng, L. Susmel, Notch static strength of additively manufactured acrylonitrile butadiene styrene (ABS), Addit. Manuf. 34 (2020), 101212, https://doi.org/10.1016/j.addma.2020.101212.
[28] T.L. Anderson, Fracture mechanics: fundamentals and applications, 4th ed., CRC Press - Taylor and Francis Group, Boca Raton, FL, 2005.
[29] F. Minami, M. Ohata, H. Shimanuki, T. Handa, S. Igi, M. Kurihara, T. Kawabata, Y. Yamashita, T. Tagawa, Y. Hagihara, Method of constraint loss correction of CTOD fracture toughness for fracture assessment of steel components, Eng. Fract. Mech. 73 (2006) 1996–2020, https://doi.org/10.1016/j.engfracmech.2006.03.013.
[30] S. Cicero, F. Gutierrez-Solana, J.A. Alvarez, Structural integrity assessment of components subjected to low constraint conditions, Eng. Fract. Mech. 75 (2008) 3038–3059, https://doi.org/10.1016/j.engfracmech.2007.12.013.
[31] S. Cicero, R.A. Ainsworth, F. Gutiérrez-Solana, Engineering approaches for the assessment of low constraint fracture conditions: a critical review, Eng. Fract. Mech. 77 (2010) 1360–1374, https://doi.org/10.1016/j.engfracmech.2010.02.026.
[32] I. Hadley, A. Horn, Treatment of constraint in BS 7910:2013, ISO 27306 and DNVGL-RP-F108, Int. J. Press. Vessel. Pip. 169 (2019) 77–93, https://doi.org/10.1016/j.ijpvp.2018.11.015.